Asian Journal of Chemistry; Vol. 38, No. 3 (2026), 610-618
ASIAN JOURNAL OF CHEMISTRY
https://doi.org/10.14233/ajchem.2026.35130

Growth and Physico-chemical Characterisation of Novel Glycine-Ammonium Bicarbonate Crystal

M. JAYACHITHRA[1], P. LALITHA[2], M. MEENA[1], D. PRAKASH[4,*], A. AJITH[4,*], R.S. SUNDARARAJAN[1], M. SHALINI[1] and T.C. SABARI GIRISUN[3]

[1]Department of Physics, Government Arts College (Autonomous), (Affiliated to Bharathidasan University, Tiruchirappalli), Kumbakonam-612001, India
[2]Department of Physics, Hindusthan Institute of Technology (Autonomous) (Affiliated to Anna University, Chennai), Coimbatore-600025, India
[3]Nanophotonics Laboratory, Department of Physics, Bharathidasan University, Tiruchirappalli-620024, India
[4]Department of Physics, Dr. Mahalingam College of Engineering and Technology, Pollachi-642003, India

*Corresponding author: E-mail: prakasphy@gmail.com

Received: 24 August 2025 *Accepted*: 20 December 2025 *Published online*: 6 March 2026 AJC-22279

At room temperature, a semi-organic single crystal of glycine coupled with ammonium bicarbonate (GABIC) was developed using a standard approach. Spectroscopic examination confirmed its composition and X-ray diffraction revealed a monoclinic structure. FT-IR spectroscopy identified functional groups, whereas UV-visible and fluorescence spectra exhibited the optical and electrical properties, including an optical band gap of 4.49 eV. Several optical metrics were measured, including the extinction coefficient and reflectance. Vickers microhardness tests validated its classification as a soft material and mechanical parameters such as hardness number and fracture toughness were measured. Scanning electron microscopy was used to analyse surface morphology and dielectric measurements were also measured. The laser-induced damage threshold of the GABIC crystal was evaluated using a Q-switched Nd:YAG laser, demonstrating its ability to withstand high optical intensities. Nonlinear optical analysis conducted through the open-aperture Z-scan technique yielded a nonlinear absorption coefficient (β) of 0.95×10^{10} m W^{-1}, confirming the strong potential of GABIC for optical limiting applications. The incorporation of glycine significantly influenced the spectral response of crystal, enhanced its optical transparency and improved its mechanical stability, thereby contributing to its multifunctional performance in advanced photonic and optoelectronic systems.

Keywords: Optical studies, Microhardness, Dielectric properties, Laser damage threshold, Nonlinear optics.

INTRODUCTION

Single-crystal growth plays a crucial role in advancing modern science and technology, particularly in the production of electronic devices [1,2]. Consequently, researchers are continuously striving to develop single crystals rapidly and cost-effectively. Nonlinear optics (NLO) is a dynamic interdisciplinary field dedicated to the development of single crystals exhibiting nonlinear optical properties and investigating their applications across diverse technologies. These include second harmonic generation (SHG) [3,4], amplitude [5] and phase modulation [6], laser technology [7,8], optical switching [9], phase matching, telecommunications [10], as well as optical communication and storage devices [11,12]. The quest for sophisticated single crystals with exceptional qualities has accelerated over the past 40 years due to their wide range of applications in microelectronics [13], semiconductors [14], photonics [15] and sensors [16]. Glycine stands out among amino acids due to its exceptional chemical versatility, which enables it to interact with both cations and anions due to its dual acid-base nature.

The majority of naturally occurring amino acids have NLO qualities, with glycine having the most basic structure but being extremely important due to its optical properties [17,18]. Glycine, a structurally versatile amino acid existing in three polymorphic crystalline forms, has been widely employed to enhance both linear and nonlinear optical properties, with its crystal growth behaviour being strongly governed by reactor configuration, solution chemistry and external growth conditions [19], making amino acids particularly suitable for the

development and investigation of nonlinear optical crystals [20,21].

This study reports the growth of glycine ammonium bicarbonate (GABIC) single crystals using the slow evaporation solution growth method. The formed crystals were extensively analysed using various techniques, including X-ray diffraction (XRD), UV-Vis-NIR spectroscopy, laser damage threshold (LDT) analysis, Fourier transform infrared (FT-IR) spectroscopy, fluorescence studies, dielectric measurements and scanning electron microscopy with energy dispersive X-ray spectroscopy (SEM-EDX). Moreover, the structural integrity, optical transmittance, defect analysis and mechanical properties were evaluated using Vickers microhardness testing.

EXPERIMENTAL

Crystal growth and material synthesis: The glycine-ammonium bicarbonate (GABIC) crystal was synthesised at room temperature using a 1:1 molar ratio of NH_4HCO_3 and glycine dissolved in deionised water. The solution was magnetically agitated for 4 h to ensure uniform mixing and the saturated solution was filtered into a beaker before being treated using the slow evaporation solution growth method to obtain high-quality and transparent crystals. Fig. 1 shows the image of the synthesized GABIC crystals.

Fig. 1. Photograph of GABIC crystal

Instrumentation: The Bruker Enraf Nonius CAD4 diffractometer was used for single-crystal X-ray diffraction (XRD). The UV-visible spectrum of the GABIC crystal was acquired at room temperature with a Perkin-Elmer Lambda 35 spectrometer in the 200-1100 nm range. Fourier transform infrared (FT-IR) spectrum was collected using a Bruker Tensor 27 spectrometer at ± 2 resolution in the mid-IR band (4000-400 cm^{-1}). Fluorescence spectrum was examined at room temperature with a Varian Cary Eclipse fluorescence spectrometer. Dielectric characteristics were evaluated using an HIOKI 3532-50 LCR HiTester at frequencies ranging from 5 Hz to 50 MHz. Surface morphology was studied at various magnifications using a Quanta FEG-250 scanning electron microscope. An Nd:YAG Q-switched laser with a pulse width of 20 ns was used to determine the laser damage threshold. The Z-scan technique was performed using a Q-switched Nd:YAG laser operating at its second harmonic wavelength of 532 nm.

RESULTS AND DISCUSSION

Single crystal X-ray diffraction: The synthesised crystal was subjected to single-crystal X-ray diffraction (sXRD) investigation with a Bruker Enraf Nonius CAD4 diffractometer, revealing a monoclinic structure. Table-1 shows the lattice properties as compared to the starting material. While the doped crystal maintains the same general structure as the base molecule, the addition of the dopant has caused slight structural changes, as shown by the modest variation in lattice characteristics between the GABIC crystal and pure glycine [22]. Despite the similarities in the crystal systems of both the parent and synthesised crystals, the introduction of the dopant has resulted in slight variations in the lattice constants (Table-1).

FTIR studies: The produced crystals were crushed into a fine powder with a mortar and pestle and examined using FT-IR spectroscopy. The presence of glycine in the NH_4HCO_3 crystal was subjectively confirmed using spectra taken in the 4000-400 cm^{-1}. Glycine ammonium bicarbonate (GABIC) crystal FT-IR spectrum is shown in Fig. 2, and a comparison of the functional group distribution in GABIC single crystal with pure glycine and other comparable crystals is presented in Table-2. The -OH stretching band at 3167 cm^{-1} shows sensitivity to hydrogen bonding in the crystal lattice, whereas the -CH stretching at 1333 cm^{-1} validates the zwitterionic form of glycine. Moreover, the -CH_3 stretching vibrations of amino acids are appear at 1450 cm^{-1}. The existence of these distinctive vibrations of doped crystals indicates that glycine impurities were successfully incorporated into the crystal structure.

Optical studies: The crystal formed by reacting glycine with NH_4HCO_3 exhibits low UV transmission, making it an excellent candidate for UV shielding applications. Furthermore, its strong transmission in the visible region suggests suitability for second harmonic generation (SHG) applications.

Fig. 3a presents the transmission and absorption curves for UV light, demonstrating that the crystal achieves over 90% optical transparency in the visible spectrum. This high transparency highlights its potential for nonlinear optical uses. The optical transmission spectrum, recorded with a UV-visible spectrometer, covers the range from 200 to 1100 nm. The crystal shows a cutoff wavelength at 240 nm and maintains good

TABLE-1
LATTICE PARAMETER FOR GROWN CRYSTAL

Crystal	a (Å)	b (Å)	c (Å)	α = β	γ	Cell volume (Å)	Crystal system
Pure glycine	5.012	11.971	5.457	90º	111.71	308.620	Monoclinic
GABIC	5.102	11.971	5.458	90º	111.70	309.698	Monoclinic

TABLE-2
COMPARISON OF IR BANDS IN GABIC AND DOPED CRYSTALS

Pure glycine [23]	Glycine ammonium bicarbonate crystal (GABIC)	Glycine doped $ZnSO_4 \cdot H_2O$ crystal [24]	Glycine doped LAHCL crystal [25]	Assignments
696	697	694	–	Carboxylate group
–	892	894	891	Stretching C-C
–	1033	1033	1051	C-C-N
1112	1112	1111	–	NH_3^+ group
–	1131	–	1131	Wagging NH_2
1311	1333	1327	–	CH stretching vibration
1492	1443	1442	1459	CH_3 bending
1554	1519	–	1519	NH_3^+ symmetric deformation
–	1590	–	1596	COO^- assymtric stretching
2126	2123	–	–	
–	2826	–	2831	CH_2 symmtric stretching
–	3168	3170	3170	O-H stretching

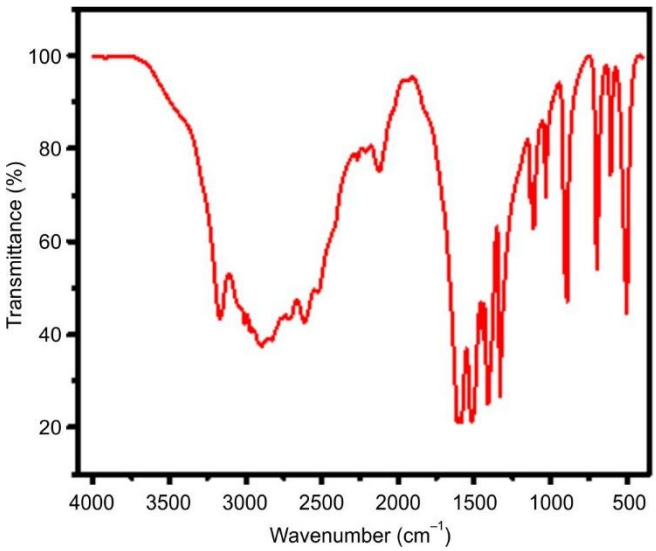

Fig. 2. FT-IR spectrum of glycine ammonium bicarbonate (GABIC)

transmittance throughout the visible range, making it ideal for the optical window applications.

The transmission data were thoroughly analysed to determine key optical parameters including transmittance, absorption, reflectance, absorption coefficient, optical band gap and refractive index. The optical absorption coefficient (α) was calculated using the following equation:

$$\alpha = \frac{1}{t}\log\left(\frac{1}{T}\right) \quad (1)$$

where T represents transmission and t is the crystal thickness. For high photon energies (hν) near the absorption edge, the crystal's absorption coefficient (α) follows the equation below, where T represents transmission; and t represents crystal thickness:

$$Ah\nu = A(h\nu - E_g)^{1/2} \quad (2)$$

After initially viewing $(\alpha h\nu)^2$ and hν, the crystalline material's band gap was calculated, as shown in Fig. 3b.

This was accomplished by extending the linear region at the energy level, yielding a correctly calculated band gap of 6.3 eV. Because of its large band gap, the glycine-ammonium bicarbonate crystal is an excellent choice for optoelectronic applications [26]. The band gap (E_g) and extinction coefficient (K) are important optical factors in determining crystal material potential. The equation below expresses the relationship between the extinction coefficient (K) and reflectance (R):

$$K = \frac{\alpha\lambda}{4\pi} \quad (3)$$

$$R = \frac{1 \pm \sqrt{1 - \exp(-xt) + \exp(\alpha t)}}{1 + \exp(-\alpha t)} \quad (4)$$

The development of optoelectronic devices can be optimised to acquire materials appropriate for device manufacture by adjusting these parameters. The change in reflectance (R) and extinction coefficient (K) with increasing photon energy is shown in Fig. 3c-d [27]. Therefore, GABIC crystal is a viable option for optical applications due to its low reflectance and extinction coefficient, which indicate that it has good transmittance [28,29].

The Urbach relation (eqn. 5) was used to determine the absorption coefficient (α) [30]. The increase in α value with incident photon energy (hν) prior to the absorption edge indicates the crystalline structure of the GABIC crystal.

The Urbach equation is given as:

$$\alpha h\nu = \alpha_0 \exp\left(\frac{h\nu}{E_u}\right) \quad (5)$$

where h denotes Planck's constant, E_u denotes the Urbach energy, which stands for depth-of-tailed levels that stretch beyond prohibited electronic territory. High crystallinity in the crystal is shown by the linear part of the plot between log α and photon energy (hν), which has a slope of 4.124 (Fig. 3e). By using the reciprocal of the slope value, the Urbach energy (E_u) was calculated to be 0.2248, however, its low value indicates that the grown GABIC crystal possesses minimal structural disorder and a low density of defects [31].

Fluorescence studies: The fluorescence spectrum recorded in the range of 235-900 nm (Fig. 4) exhibited prominent blue emission peaks at 449.64 and 484.71 nm, while a comparatively weaker emission observed at 520.69 nm, attributed to the metal-related interactions, confirmed the presence of greenish luminescence. These transitions are equivalent to π–π* electronic transitions. Furthermore, the peaks at 660.03 nm

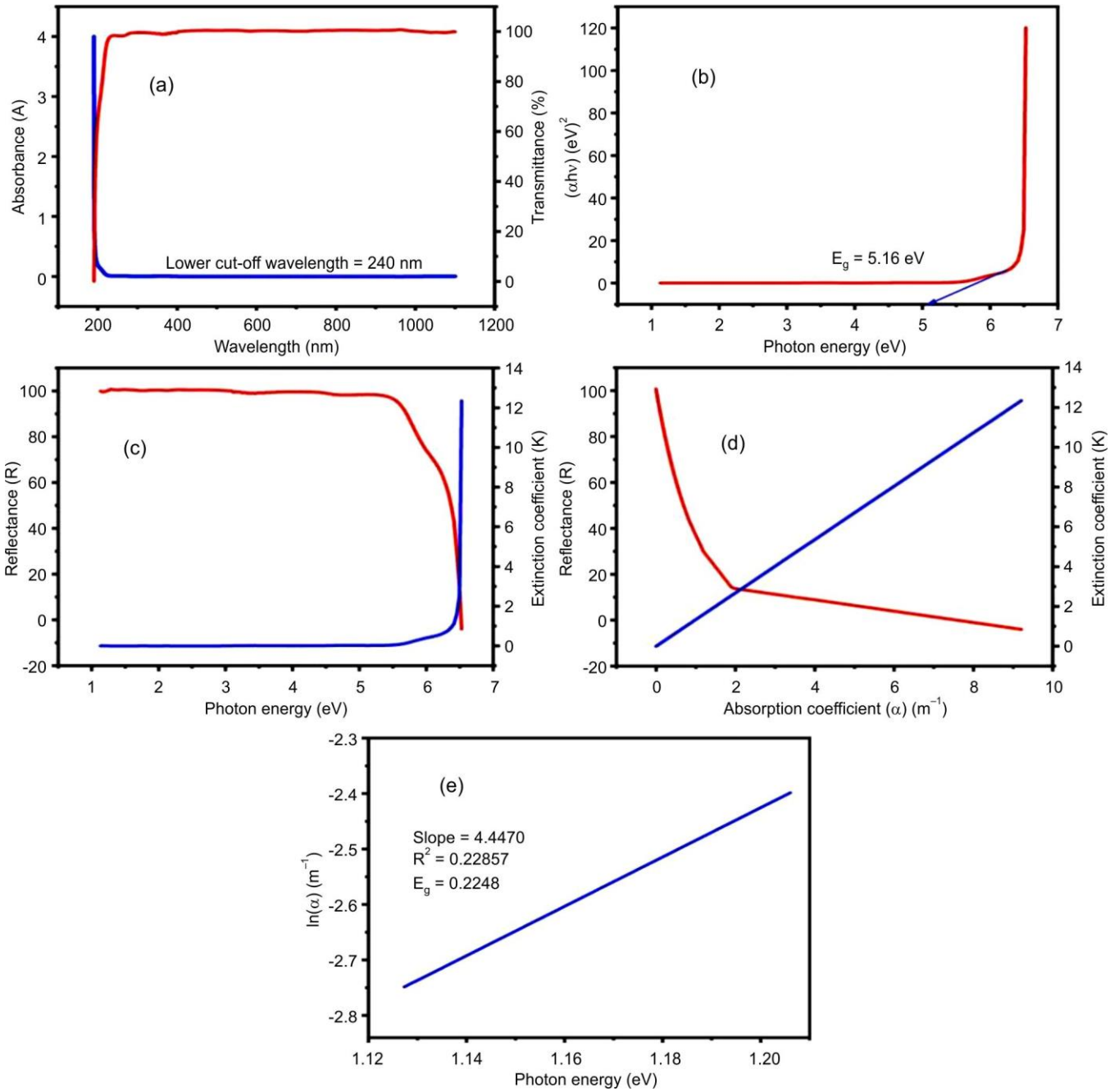

Fig. 3. (a) Absorbance and transmittance curves, (b) photon energy (eV) *versus* (αhν) $(eV)^2$, (c) photon energy (eV) *versus* extinction coefficient (K), reflectance (R), (d) variation of absorption coefficient (α) with reflectance (R), extinction coefficient (K) and (e) plot eV *versus* ln (α)

and 668.32 nm correspond to red light emission indicating a low-energy transition level impacted by the surrounding environment. This effect causes high fluorescence emission in the red area.

Vicker micro hardness analysis: Vickers microhardness testing was used to assess the mechanical properties of the crystals and all static indentation measurements were taken at room temperature at the interval period of 10 s. The tests were conducted on defect-free crystals with smooth and flat surfaces. The crystal was securely fastened to the base of the microscope to provide the stability during the indentation procedure. Indentations were precisely produced with loads ranging from 25 to 100 g. As the applied pressure increased to 100 g, cracks appeared around the indentation point, illustrating the material's response to increased stress (Fig. 5).

The Vickers microhardness (H_v) was determined using the following formula:

$$H_v = \frac{1.8544P}{d^2} (Kg/mm^2) \quad (6)$$

where Vickers hardness (H_v) was measured in G Nm^{-2}, penetration force (P) was measured in N and indentations diagonal length (d) was measured in m.

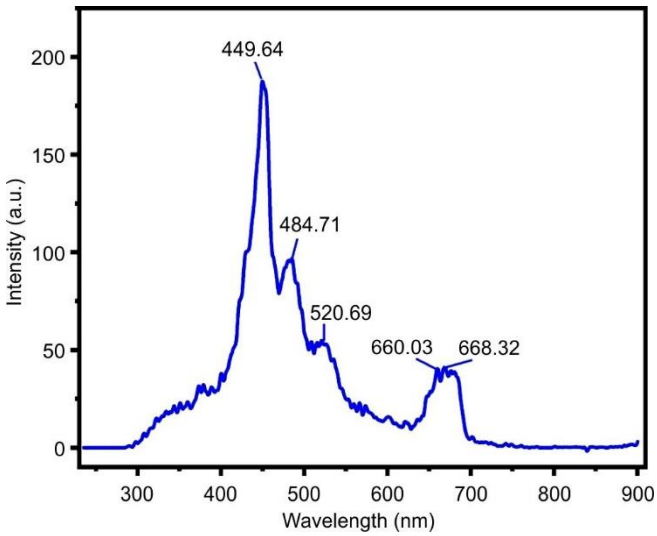

Fig. 4. Fluorescence spectrum of GABIC crystal

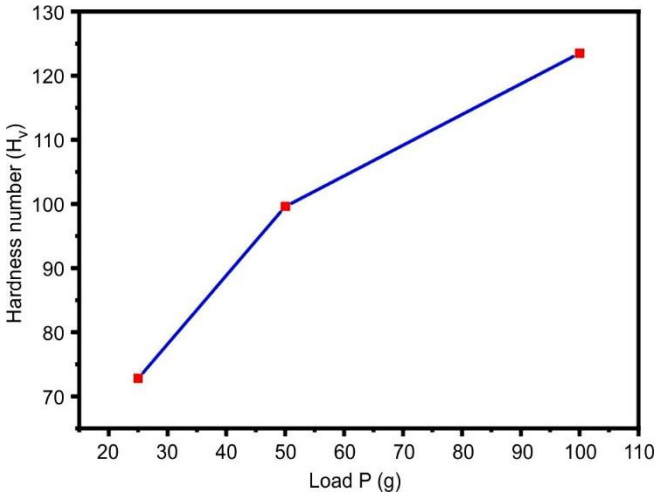

Fig. 5. Plot of the Vickers hardness number and the applied load

Fig. 5 depicts the relationship between Vickers hardness number and applied load. A linear correlation between log P and log d was observed (Fig. 5), yielding a Meyer's index value of n = 3.18, and since n > 2, the grown crystal can be classified as mechanically soft.

The yield strength (σ_y) was derived from the hardness value using eqn. 7 [32]:

$$\sigma_y = \frac{H_v}{3}(N/m^2) \quad (7)$$

Using Wooster's law, the elastic stiffness constant (C_{11}) was calculated empirically.

$$C_{11} = (H_v)^{7/4} \quad (8)$$

In addition to material toughness, fracture toughness (K_c) quantifies a material's ability to resist crack propagation under continuous stress. This property plays a crucial role in determining the mechanical stability of the material. The fracture toughness was calculated using eqn. 9:

$$K_c = \frac{P}{(\beta C)^{2/3-}} \quad (9)$$

The crack length (C), measured from the indentation center to the crack tip, corresponds to the Vickers indenter constant, which is set at 7.

Another essential mechanical characteristic is brittleness, which defines the material's tendency to fracture under stress without significant plastic deformation. The brittleness index (Bi) was calculated using eqn. 10:

$$Bi = \frac{H_v}{K_c} \quad (10)$$

The parameters, such as yield strength (σ_y), brittleness index (Bi), stiffness constant (C_{11}) and fracture toughness (K_c), are listed in Table-3 under various loads (P) [33].

Dielectric studies: A dielectric characteristics of the material provide information about the polarisation mechanisms, the behaviour of electric field at the atomic level and the general quality. The polarisation effects are reflected in the movement of charges within the material. Eqns. 11 and 12 was used to calculate the dielectric loss (ε'') and dielectric constant (ε'):

$$\varepsilon' = \frac{C \times d}{\varepsilon_0 A} \quad (11)$$

$$\varepsilon'' = \varepsilon' \tan\delta \quad (12)$$

where d represents the thickness of crystal; C is the capacitance; and A is the surface area. The relationship among the electronic, ionic, orientational and space-charge polarizations accounts for the observed decrease in dielectric constant with increasing frequency. These two depict the relationship between the two frequencies (Fig. 6a-b). Furthermore, the ε' decreases significantly as the frequency increases. In addition to the impurity dipoles, thermally generated charge carriers are responsible for the majority of the surge in high frequency. Similarly, dielectric loss reduces with frequency, as shown in Fig. 6b. At lower frequencies, the dielectric loss increases due to space-charge polarization, which is strongly affected by the purity and structural perfection of the crystal, while its overall magnitude is governed by the frequency-squared dependence of dielectric loss.

SEM studies: The surface morphology of GABIC crystals was examined using a scanning electron microscope (SEM), as shown in Fig. 7. The incorporation of NH_4HCO_3 into the glycine matrix resulted in the significant changes to the surface structure, producing smooth and defect-free crystal surfaces. However, the doping process slightly reduced the mechanical

TABLE-3
CALCULATED PARAMETER OF GABIC CRYSTAL

Load P (g)	H_v (kg mm^{-2})	N	σ_y (GPa)	C_{11} (GPa)	K_c (kg m$^{-3/2}$)	Bi × 10^5
25	18.14	3.18	24.26	18.14	8.26	8.41
50	31.40	3.18	33.20	31.40	11.52	22.14
100	45.75	3.18	41.16	45.75	23.70	48.52

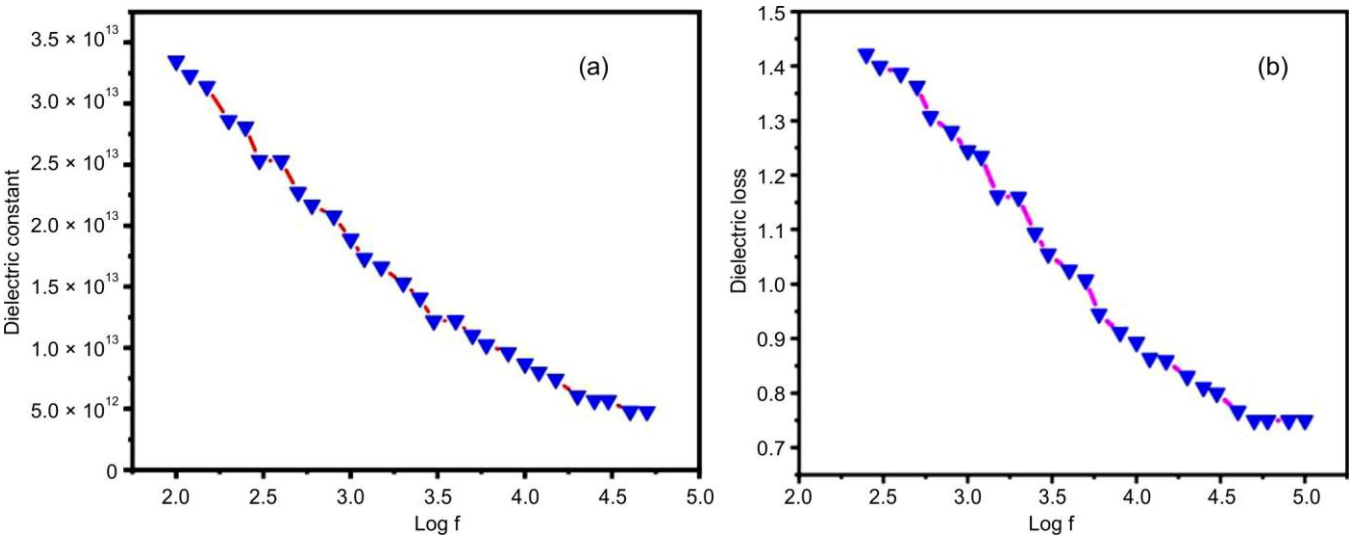

Fig. 6. (a) Dielectric constant *vs.* log frequency for GABIC and (b) dielectric loss *vs.* log for GABIC

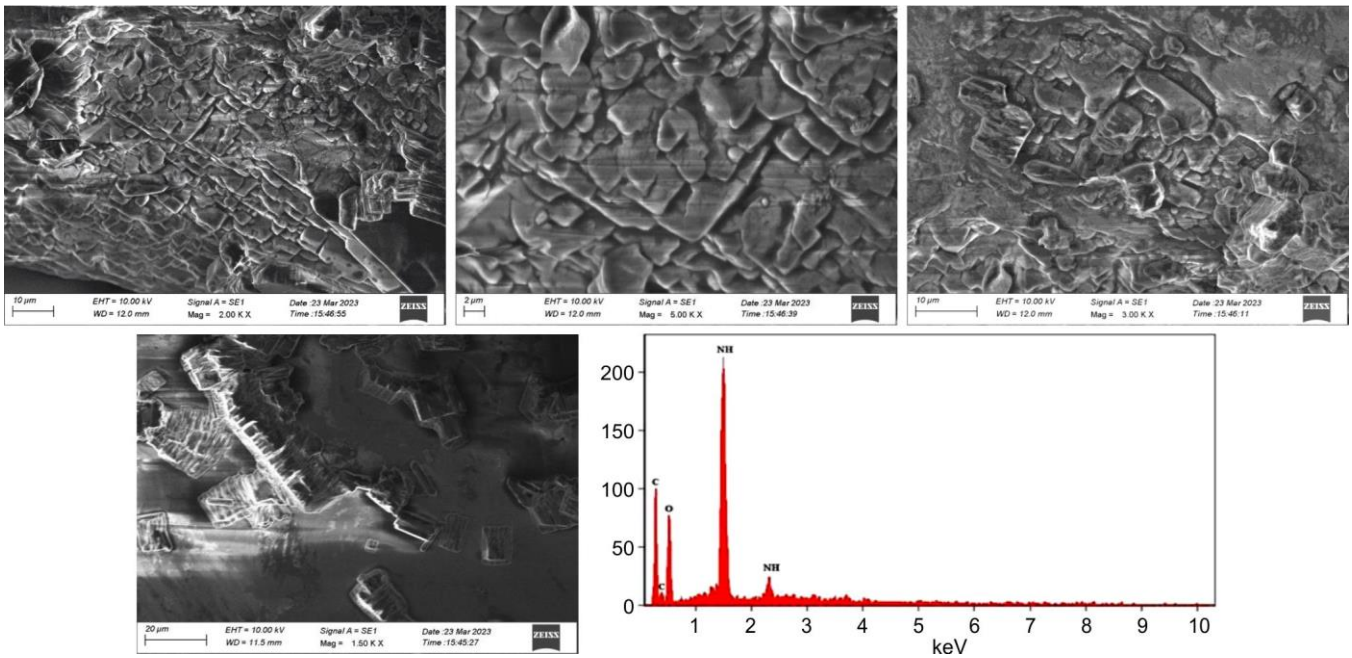

Fig. 7. Morphological analysis of GABIC crystal

strength of the material. Despite this, the high-quality surface morphology makes GABIC crystals suitable for various opto-electronic applications. The accompanying energy dispersive X-ray (EDX) analysis further confirmed the successful incorporation of ammonium ions into the glycine crystal lattice, as evidenced by the presence of characteristic elemental peaks.

Laser damage threshold (LDT) studies: A key factor restricting the practical use of optical crystals is their optical damage threshold. To evaluate this, the experiments were conducted on sample crystals using a Q-switched Nd:YAG laser with a pulse width of 10 ns and a repetition rate of 10 Hz. A laser damage threshold of 37.04 GW/cm^2 was achieved by gradually increasing the focus along the optical axis while guiding the beam. The current findings verified that this threshold exceeds the energy levels required to cause fractures on the crystal surface. Analysis of both the laser beam energy and resulting damage confirmed that this threshold surpasses the energy required to induce surface cracks. Remarkably, this number exceeds that reported for the different nonlinear optical (NLO) materials, listed in Table-4, emphasizing its importance.

Z-Scan evaluation and optical limiting studies: Proposed by Sheik-Bahae *et al.* [40], the Z-scan method is widely employed to characterize third-order optical non-linearities, particularly the nonlinear absorption coefficient of materials. This technique involves exciting the sample molecules with a Gaussian laser beam propagating along the Z-axis.

In this experiment, a Q-switched Nd:YAG laser operating at the second harmonic wavelength of 532 nm with an average pulse energy of 200 μJ was used. A convex len focused the laser beam, defining the focal point (where fluence is highest) as Z = 0. The GABIC sample was diluted in ethanol

TABLE-4
COMPARISON OF LASER DAMAGE THRESHOLD (LDT) VALUE OF GABIC CRYSTAL WITH OTHER REPORTED CRYSTALS

Crystal	LDT values (GW cm^{-2})	Ref.
Glycine ammonium bicarbonate	37.04	Present work
L-Methionine hydrogen phthalate	23.12	[34]
L-Alanine sodium nitrate	14.51	[35]
L-Proline cadmium chloride	4.747	[36]
2-Amino-5-nitropyridinium nitrate (2A5NPN)	4	[37]
Potassium titanyl phosphate (KTP)	> 1.5-2.2	[38]
2-Amino-5-nitropyridine 4-chlorobenzoic (2A5NP4CBA)	6.2	[39]

to achieve a linear transmittance of approximately 70% and placed in a 1 mm thick quartz cuvette. The sample was then moved precisely along the Z-axis, toward and away from the focal point, using a computer-controlled stage, while the transmitted intensity was recorded at various positions. Depending on its position relative to the focus, the sample transmitted more or less, which is attributed to light-induced nonlinear effects [41,42].

The transmittance data at each Z-position were also analysed following the method proposed by Sheik Bahae *et al.* [40]. The experimental Z-scan results were fitted to established nonlinear optical models to extract the relevant nonlinear optical coefficients. The equation used to determine the material's nonlinear absorption coefficient is shown as:

$$\frac{dI}{dz'} = \left(\frac{\alpha_0}{(1 + I/I_S)} + \beta I \right) I \qquad (13)$$

where I is the laser intensity; β is the effective nonlinear absorption coefficient; and α_0 is the linear absorption coefficient of the material. The open-aperture Z-scan curve (Fig. 8a) shows a decrease in transmittance as the sample approaches the focal point, characterised by a pronounced valley indicative of reverse saturable absorption. The experimental data best fit a two-photon absorption (2PA) mechanism. Here, β represents the effective 2PA coefficient, accounting for both genuine and sequential two-photon absorption contributions. The nonlinear parameters, including the saturation intensity (I_s) and β, were calculated from the best-fit curve. For the title compound, these values were estimated as $I_s = 62 \times 10^{11}$ W m^2; $\beta = 0.95 \times 10^{-10}$ M W^{-1}.

Optical absorption and emission studies revealed that GABIC exhibits a strong UV absorption band at 240 nm and multiple visible emission peaks at 450, 485, 521, 660 and 668 nm. When excited with a green laser, these emissions act as a two-photon absorption state at 240 nm and a near-resonant state at 521 nm, enabling successive two-photon absorption including excited-state absorption. This means GABIC undergoes sequential two-photon absorption, where the first photon excites electrons to the green emission state and the second photon further elevates them to the UV band. This unique nonlinear absorption, driven by excited-state absorption, is the foundation of the compound's optical limiting behaviour.

To further analyse the optical limiting properties, the energy flux, expressed as input fluence, was examined. Fig. 8b displays the energy distribution of the photon beam as a function of normalised transmittance, derived from the Z-scan measurements. Eqn. 14 was to determine the fluence (F(z)):

$$F(z) = \left[4\sqrt{\ln(2)} \left(\frac{E_{in}}{\pi^{3/2}} \right) \right] / \omega(z)^2 \qquad (14)$$

where E_{in} represents the laser energy and F(z) denotes the input fluence [43]. The optical limiting curve clearly demons-

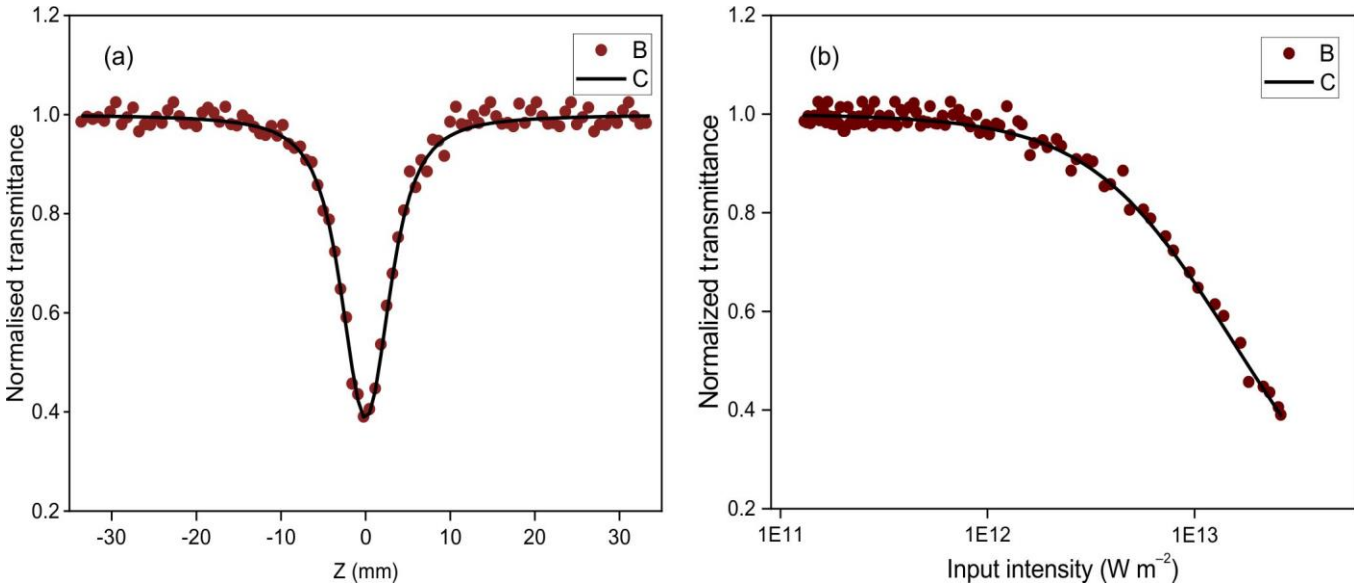

Fig. 8. (a) Normalized transmittance with an open aperture as a function of Z position and (b) optical limiting curve for GABIC

trates the nonlinear optical behaviour of the system. Effective optical limiting performance requires materials with a low onset optical limiting threshold, which corresponds to the energy level at which nonlinear effects begin to manifest. For GABIC, the onset optical limiting threshold was determined to be 3.26×10^{12} W m^{-2}. The characteristics of the optical limiting curve suggest that the strong excited state absorption (ESA) behaviour of GABIC crystals and contributes significantly to its optical limiting capabilities. This nonlinear optical power limitation phenomenon restricts the output light intensity, making the material an effective optical limiter. Such materials are essential for protecting the photosensitive components from laser-induced damage.

Conclusion

High-purity glycine ammonium bicarbonate (GABIC) single crystals were successfully grown at room temperature using the slow evaporation method. XRD analysis confirmed that the crystal retained the monoclinic structure of the starting material, with only minor changes in cell parameters resulting in a slight volume variation. The optical spectral analysis revealed an optical band gap of 5.16 eV and enhanced optical constants. Fluorescence studies further demonstrated the high crystalline quality of the grown GABIC crystal, with a prominent blue emission peak observed at 449.69 nm. Mechanical stability and structural integrity were assessed *via* Vickers microhardness testing. The third-order nonlinear absorption coefficient was determined using the open-aperture Z-scan technique, while optical limiting experiments confirmed the suitability of GABIC crystal for such applications. Moreover, laser damage threshold (LDT) measurements validated the robustness of GABIC crystal, highlighting its promise for diverse optoelectronic applications.

CONFLICT OF INTEREST

The authors declare that there is no conflict of interests regarding the publication of this article.

DECLARATION OF AI-ASSISTED TECHNOLOGIES

During the preparation of this manuscript, the authors used an AI-assisted tool(s) to improve the language. The authors reviewed and edited the content and take full responsibility for the published work.

REFERENCES

1. S. Min, T.-S. Kim, Y. Lee, H. Cho, W. Xu and T.-W. Lee, *Small*, **11**, 45 (2015); https://doi.org/10.1002/smll.201401487
2. D.A. Pinnow, L.G. VanUitert, A.W. Warner and W.A. Bonner, *Appl. Phys. Lett.*, **15**, 83 (1969); https://doi.org/10.1063/1.1652917
3. Y. Fu, Z. Liu, S. Yue, K. Zhang, R. Wang and Z. Zhang, *Nanomaterials*, **14**, 662 (2024); https://doi.org/10.3390/nano14080662
4. H. Hirori, A. Doi, F. Blanchard and K. Tanaka, *Appl. Phys. Lett.*, **98**, 091106 (2011); https://doi.org/10.1063/1.3560062
5. S.A. De Vries, P. Goedtkindt, S.L. Bennett, W.J. Huisman, J.J. De Yoreo, M.J. Zwanenburg, D.-M. Smilgies, W.J.P. Van Enckevort, P. Bennema and E. Vlieg, *Phys. Rev. Lett.*, **80**, 2229 (1998); https://doi.org/10.1103/PhysRevLett.80.2229
6. J. Cao, E. Ertekin, V. Srinivasan, W. Fan, S. Huang, H. Zheng, J.W.L. Yim, D.R. Khanal, D.F. Ogletree, J.C. Grossman and J. Wu, *Nat. Nanotechnol.*, **4**, 732 (2009); https://doi.org/10.1038/nnano.2009.266
7. M. Anis, R.N. Shaikh, M.D. Shirsat and S.S. Hussaini, *Opt. Laser Technol.*, **60**, 124 (2014); https://doi.org/10.1016/j.optlastec.2014.01.011
8. W.-J. Xu, C.-T. He, C.-M. Ji, S.-L. Chen, R.-K. Huang, R.-B. Lin, W. Xue, J.-H. Luo, W.-X. Zhang and X.-M. Chen, *Adv. Mater.*, **28**, 5886 (2016); https://doi.org/10.1002/adma.201600895
9. A.J. Almosawe and H.L. Saadon, *Chin. Opt. Lett.*, **11**, 041902 (2013); https://doi.org/10.3788/COL201311.041902
10. W. Zhang, H. Yu, H. Wu and P.S. Halasyamani, *Chem. Mater.*, **29**, 2655 (2017); https://doi.org/10.1021/acs.chemmater.7b00243
11. W. Zeng, L. Shu, Q. Li, S. Chen, F. Wang and X.-M. Tao, *Adv. Mater.*, **26**, 5310 (2014); https://doi.org/10.1002/adma.201400633
12. M. Nikl and A. Yoshikawa, *Adv. Opt. Mater.*, **3**, 463 (2015); https://doi.org/10.1002/adom.201400571
13. S. Kawata and Y. Kawata, *Chem. Rev.*, **100**, 1777 (2000); https://doi.org/10.1021/cr980073p
14. A.L. Briseno, J. Aizenberg, Y.-J. Han, R.A. Penkala, H. Moon, A.J. Lovinger, C. Kloc and Z. Bao, *J. Am. Chem. Soc.*, **127**, 12164 (2005); https://doi.org/10.1021/ja052919u
15. M.I. Baig, M. Anis, S. Kalainathan, B. Babu and G.G. Muley, *Mater. Technol.*, **32**, 560 (2017); https://doi.org/10.1080/10667857.2017.1321275
16. R.N. Shaikh, M. Anis, M.D. Shirsat and S.S. Hussaini, *Optik*, **154**, 435 (2018); https://doi.org/10.1016/j.ijleo.2017.10.107
17. T. Kar, *Prog. Cryst. Growth Charact. Mater.*, **58**, 74 (2012); https://doi.org/10.1016/j.pcrysgrow.2012.03.002
18. P. Jananakumar and P. Mani, *Indian J. Appl. Phys.*, **53**, 819 (2015).
19. P.S. Zelenovskii, D.S. Vasileva, S.G. Vasilev, S. Kopyl and A. Kholkin, *Front. Mater.*, **9**, 918890 (2022); https://doi.org/10.3389/fmats.2022.918890
20. K. Ambujam, K. Rajarajan, S. Selvakumar, I. Vetha Potheher, G.P. Joseph and P. Sagayaraj, *J. Cryst. Growth*, **286**, 440 (2006); https://doi.org/10.1016/j.jcrysgro.2005.10.013
21. R.M. Kumar, D.R. Babu, D. Jayaraman, R. Jayavel and K. Kitamura, *J. Cryst. Growth*, **275**, 1935 (2005); https://doi.org/10.1016/j.jcrysgro.2004.11.260
22. P.J. Angelin and P.S. Premkumar, *Chem. Inorg. Mater.*, **3**, 100060 (2024); https://doi.org/10.1016/j.cinorg.2024.100060
23. S. Kumar, A.K. Rai, V.B. Singh and S.B. Rai, *Spectrochim. Acta A: Mol. Biomol. Spectrosc.*, **61**, 2741 (2005); https://doi.org/10.1016/j.saa.2004.09.029
24. P. Sagunthala, V. Veeravazhuthi, P. Hemalatha and P. Yasotha, *Ferroelectrics*, **504**, 96 (2016); https://doi.org/10.1080/00150193.2016.1239487
25. K. Sangeetha, R.R. Babu, G. Bhagavannarayana and K. Ramamurthi, *Spectrochim. Acta A Mol. Biomol. Spectrosc.*, **79**, 1017 (2011); https://doi.org/10.1016/j.saa.2011.04.014
26. R.N. Shaikh, M. Anis, A.B. Gambhire, M.D. Shirsat and S.S. Hussaini, *Mater. Res. Express*, **1**, 015016 (2014); https://doi.org/10.1088/2053-1591/1/1/015016
27. M. Meena, M. Shalini, B.S. Ebinezer, R.S. Sundararajan, T.C. Sabari Girisun and E. Manikandan, *J. Mater. Sci. Mater. Electron.*, **34**, 1778 (2023); https://doi.org/10.1007/s10854-023-11195-y
28. C.J. Raj, S. Dinakaran, S. Krishnan, B. Milton Boaz, R. Robert and S.J. Das, *Opt. Commun.*, **281**, 2285 (2008); https://doi.org/10.1016/j.optcom.2007.12.019
29. V. Venkataramanan, S. Maheswaran, J.N. Sherwood and H.L. Bhat, *J. Cryst. Growth*, **179**, 605 (1997); https://doi.org/10.1016/S0022-0248(97)00137-1

30. F. Urbach, *Phys. Rev.*, **92**, 1324 (1953); https://doi.org/10.1103/PhysRev.92.1324
31. M.P. Mohamed, P. Jayaprakash, M. Nageshwari, C.R. Thaya Kumari, P. Sangeetha, S. Sudha, G. Mani and M. Lydia Caroline, *J. Mol. Struct.*, **1141**, 551 (2017); https://doi.org/10.1016/j.molstruc.2017.04.002
32. B. Deepa and P. Philominathan, *Optik*, **127**, 8698 (2016); https://doi.org/10.1016/j.ijleo.2016.06.073
33. S.P. Rathee and D.S. Ahlawat, *Optik*, **136**, 249 (2017); https://doi.org/10.1016/j.ijleo.2017.02.045
34. M. Shalini, R.S. Sundararajan, T.C.S. Girisun, E. Manikandan and M. Meena, *J. Mater. Sci. Mater. Electron.*, **33**, 19004 (2022); https://doi.org/10.1007/s10854-022-08733-5
35. K. Sethuraman, R. Ramesh Babu, R. Gopalakrishnan and P. Ramasamy, *Cryst. Growth Des.*, **8**, 1863 (2008); https://doi.org/10.1021/cg700965d
36. M. Shakir, S.K. Kushwaha, K.K. Maurya, R.C. Bhatt, Rashmi, M.A. Wahab and G. Bhagavannarayana, *Mater. Chem. Phys.*, **120**, 566 (2010); https://doi.org/10.1016/j.matchemphys.2009.12.008
37. V. Sivasubramani, M. Senthil Pandian, K. Boopathi and P. Ramasamy, *Mater. Res. Innov.*, **22**, 128 (2018); https://doi.org/10.1080/14328917.2016.1264859
38. D.J. Daniel and P. Ramasamy, *Opt. Mater.*, **36**, 971 (2014); https://doi.org/10.1016/j.optmat.2014.01.004
39. M. Sheik-Bahae, A.A. Said and E.W. Van Stryland, *Opt. Lett.*, **14**, 955 (1989); https://doi.org/10.1364/OL.14.000955
40. A.A. Sheik-Bahae, T.H. Said, D.J. Wei, D.J. Hagan and E.W. Van Stryland, *IEEE J. Quantum Electron.*, **26**, 760 (1990); https://doi.org/10.1109/3.53394
41. G. Muruganandi, M. Saravanan, G. Vinitha, M.B. Jessie Raj and T.C. Sabari Girisun, *Chem. Phys.*, **488-489**, 55 (2017); https://doi.org/10.1016/j.chemphys.2017.03.002
42. T.A. Hegde, A. Dutta, T.C. Sabari Girisun, M. Abith and G. Vinitha, *J. Mater. Sci. Mater. Electron.*, **30**, 18885 (2019); https://doi.org/10.1007/s10854-019-02245-5
43. A.A. Habeeba, M. Saravanan, T.C.S. Girisun and S. Anandan, *J. Mol. Struct.*, **1240**, 130559 (2021); https://doi.org/10.1016/j.molstruc.2021.130559